Annals of Biomedical Engineering, Vol. 40, No. 5, May 2012 (© 2011) pp. 1160–1169
DOI: 10.1007/s10439-011-0493-0

Altered Lung Motion is a Sensitive Indicator of Regional Lung Disease

ANDREAS FOURAS,[1] BETH J. ALLISON,[2] MARCUS J. KITCHEN,[3] STEPHEN DUBSKY,[1,4] JAYNE NGUYEN,[1,4] KERRY HOURIGAN,[1,4] KAREN K. W. SIU,[3] ROB A. LEWIS,[3] MEGAN J. WALLACE,[2] and STUART B. HOOPER[2]

[1]Division of Biological Engineering, Monash University, Clayton, VIC 3800, Australia; [2]Ritchie Centre, Monash Institute of Medical Research, Monash University, Clayton, VIC 3800, Australia; [3]School of Physics, Monash University, Clayton, VIC 3800, Australia; and [4]Department of Mechanical and Aerospace Engineering, Monash University, Clayton, VIC 3800, Australia

(*Received 24 June 2011; accepted 15 December 2011; published online 22 December 2011*)

Associate Editor Kenneth R. Lutchen oversaw the review of this article.

Abstract—Since lung diseases adversely affect airflow during breathing, they must also alter normal lung motion, which can be exploited to detect these diseases. However, standard imaging techniques such as CT and MRI imaging during breath-holds provide little or no information on lung motion and cannot detect diseases that cause subtle changes in lung structure. Phase-contrast X-ray imaging provides images of high contrast and spatial resolution with temporal resolutions that allow multiple images to be acquired throughout the respiratory cycle. Using X-ray phase-contrast imaging, coupled with velocimetry, we have measured lung tissue movement and determined velocity fields that define speed and direction of regional lung motion throughout a breath in normal Balb/c nude male mice and mice exposed to bleomycin. Regional maps of lung tissue motion reveal both the heterogeneity of normal lung motion, as well as abnormal motion induced by bleomycin treatment. Analysed histologically, bleomycin treatment caused pathological changes in lung structure that were heterogenous, occupying less than 12% of the lung at 6 days after treatment. Moreover, plethysmography failed to detect significant changes in compliance at either 36 h or 6 days after treatment. Detailed analysis of the vector fields demonstrated major differences ($p < 0.001$) in regional lung motion between control and bleomycin-treated mice at both 36 h and 6 days after treatment. The results of this study demonstrate that X-ray phase-contrast imaging, coupled with velocimetry, can detect early stage, subtle and non-uniform lung disease.

Keywords—Velocimetry, Functional imaging, Lung disease, Lung function.

INTRODUCTION

Lung diseases restrict airflow into or out of the lungs either by increasing airway resistance or by altering lung structure, which in turn changes the elasto-mechanical and aero-resistive properties of the lung.[18,45] For example, interstitial fibrosis increases distal airway stiffness, asthma increases airway resistance and emphysema reduces lung tissue recoil thereby increasing its compliance. Although these diseases differ markedly in both cause and consequence, they all alter the mechanical properties of diseased regions and, therefore, must also alter motion of these regions.[5–7,36]

Little is known about the dynamics of lung motion during respiration, particularly how different regions of the lung move in relation to other regions during both inspiration and expiration. It is not known whether the lung expands and deflates uniformly, or whether specific regions lead or trail other regions due to differences in local compliances or proximity to the diaphragm. Similarly, it is unknown how diseases affect regional lung motion and whether motion in healthy regions is altered to compensate for diseased regions. Although this information is best provided by imaging the lung *in situ*, until recently it has not been possible to image the lung with sufficient spatial and temporal resolution.

Previous techniques to measure lung motion have relied on the surgical placement of markers,[17] inhalation of contrast agents[43] or removal of the chest wall for imaging.[4,30] More recently,[48] X-ray CT[42] techniques have been developed to assist in radiotherapy treatment planning[14,15] or the development of lung biomechanical models.[57] These methods are also capable of regional expansion measurement. However, these approaches are limited, particularly by the need to image the lung while it is stationary to minimise blurring. Thus, interpolation is required to deduce lung

Address correspondence to Andreas Fouras, Division of Biological Engineering, Monash University, Clayton, VIC 3800, Australia. Electronic mail: Andreas.Fouras@monash.edu

motion between two steady state conditions within a breath and such methods assume that the motion follows a linear or defined path.

Clinical gated 4D-CT has also been used for measurement of lung function, including expansion,[8,15] using traditional absorption based imaging at the expense of significant levels of radiation dose. Typically, the phase matching is performed to an accuracy of 7.1% of the breath cycle, or 400 ms.[40] This results in poor temporal resolution for investigation of the dynamic patterns of motion and expansion within the lung, particularly for small animal studies.

Magnetic resonance imaging has been used for 3D lung imaging and also motion measurement,[50,51] with the advantage of no radiation dose. However, the limitations of MRI methods resulted in poor spatial and temporal resolution (5 mm and 0.5 frames per second) when compared to X-ray methods.

Despite these advances in lung imaging, altered patterns of lung motion have not, to our knowledge, been utilised for disease detection.

Although standard X-ray imaging has the capacity to identify diseased regions of the lung, substantial changes in lung tissue characteristics are required to provide sufficient contrast (e.g., changes in X-ray absorption) between diseased and healthy regions.[16] Thus, standard imaging techniques offer little benefit in identifying diseased airways that exhibit subtle changes in structure, such as that which occurs during the early stages of disease. To improve the detection, assessment and management of most lung diseases, there is a need to develop techniques that provide accurate measures of regional lung function.

Phase-contrast X-ray imaging (PCXI)[47,55] exploits the phase change caused by X-ray refraction when passing between media of differing refractive indices to produce high contrast images of the lung.[19,20,27,28,56] Interference between transmitted and refracted X-rays produces high contrast images of the air/tissue boundaries compared with conventional X-ray absorption techniques[35] (Fig. 1). It is able to achieve this because the phase shift of the X-rays is generally more than three orders of magnitude greater than the absorption over the diagnostic X-ray energy range (20–90 keV). An important consequence of this is that phase-contrast images can be recorded with significantly lower dose than conventional images,[34] which is particularly important for both longitudinal studies and dynamic studies where repeated imaging is required.[35] We direct the reader to a number of topical examples of the use of PCXI[49,54] as well as some excellent review articles.[1,53]

In this study, we demonstrate that the combination of PCXI and velocimetry can produce quantitative measures of regional lung motion, which can be used to differentiate between normal and abnormal lung tissue. Furthermore, we demonstrate that this technology is more sensitive and provides richer quantitative information for disease detection than other conventional measures such as global lung function tests and non-biased histological sampling.

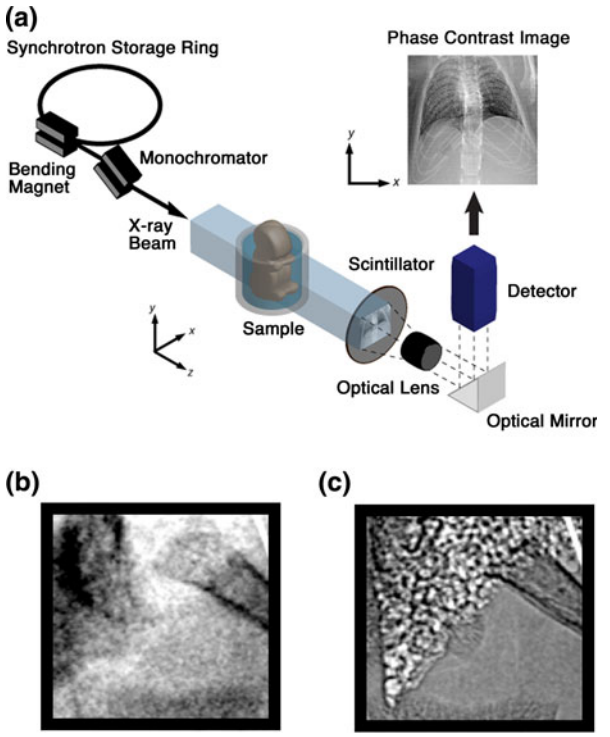

FIGURE 1. Schematic diagrams showing PCXI. (a) Schematic diagram of the imaging configuration used by the authors at the SPring-8 synchrotron. Example of the possible increase (b) and (c) in contrast for lung tissue obtained through phase-contrast X-ray imaging over absorption-based X-ray imaging (b, c—modified from Lewis *et al.*[35]).

Since lung tissue motion is complex, dynamic and heterogeneous, we have developed a novel application of the mathematical concept of divergence. We have demonstrated that despite the two-dimensional nature of the imaging described here, the divergence measure is highly correlated to changes in lung volume. This measure was evaluated in a Bleomycin-induced lung injury model in immuno-deficient Balb/c nude mice that are known to have a reduced inflammatory response to bleomycin compared to other strains.[52] Furthermore, we examined mice at 36 h and 6 days after treatment to examine the early stages of disease and determine whether we can detect disease progression.

MATERIALS AND METHODS

Protocol

All procedures were approved by the SPring-8 Synchrotron Facility and Monash University's School

of Biomedical Science's Animal Ethics Committees. Adolescent Balb/c nude male mice were exposed to bleomycin (20 mg/kg in 20 μL saline; $n = 8$; Sigma-Aldrich, Australia) or saline (20 μL; $n = 6$) by intranasal instillation and lung function was tested daily using whole body plethysmography.[39] Mice were imaged at 36 h ($n = 4$) or 6 days ($n = 4$) after treatment. For imaging, mice were anesthetized (Pentobarbital; 15 mg/kg i.p.), muscle relaxed (Pancuronium 1 mg/kg i.m.), intubated and placed in a prewarmed (37 °C) water-filled plethysmograph.[46] During imaging, mice were ventilated using a custom-designed ventilator[29] at a peak inspiratory pressure of 20 cmH_2O and end expiratory pressure of 2 cmH_2O. Inspiration and expiration times were 2.5 and 1.5 s, respectively. Although this is significantly less than the normal ventilation rate for free-breathing mice, the imaging procedures only lasted for five breaths (20 s) and was not expected to result in hypoxia or any changes in lung mechanics for these somnolent mice. Following imaging, mice were killed (Pentobarbital; 100 mg/kg i.p.) and the lungs fixed (in 10% formalin) *via* the airways at a distending pressure of 20 cmH_2O. Paraffin-embedded sections (5 μm) were stained with Massons Trichrome and used for histological analysis. Five fields of view were chosen at random from at least three randomly selected sections per mouse to measure the relative volume density of abnormal parenchymal lung regions. Then a subset analysis[22] was performed to compare the relative tissue volume in normal and abnormal parenchymal regions using an unpaired *T*-test.

Phase-Contrast X-Ray Imaging

Studies were conducted in experimental hutch 3 of BL20B2 at the SPring-8 synchrotron in Japan. The beamline consists of a bending magnet insertion device and Si-111 crystal monochromator, which generates a bright monochromatic X-ray beam. The X-ray beam transmits through the sample onto a scintillator, which converts the X-rays to visible light to be imaged by an optical detector system. Imaging was conducted at 25 keV with a sample-to-detector distance of 2 m. Images were acquired using an X-ray Converter (Hamamatsu, BM5) and an EMCCD (Hamamatsu, C9100-02) camera (Fig. 1), with an effective pixel size of 19.0 μm. Image acquisition occurred at 29 frames per second (an exposure time of 20 ms with a 14.5 ms delay between exposures, corresponding to 34.5 ms between the start of frame acquisitions) and was synchronized with ventilation to acquire 70 frames during the first part of inspiration and 30 frames during the first part of expiration for each breath. The mice were imaged in the upright position with all images acquired to obtain a frontal view of the entire thorax without the need for scanning or tiling. In all images (Fig. 2, Movie) the images are displayed without intensity inversion or laterally flipping and hence appear opposite in both regards in comparison to clinical X-ray images.

Velocimetry

The velocimetric analysis employed to measure lung motion is based on particle image velocimetry (PIV);

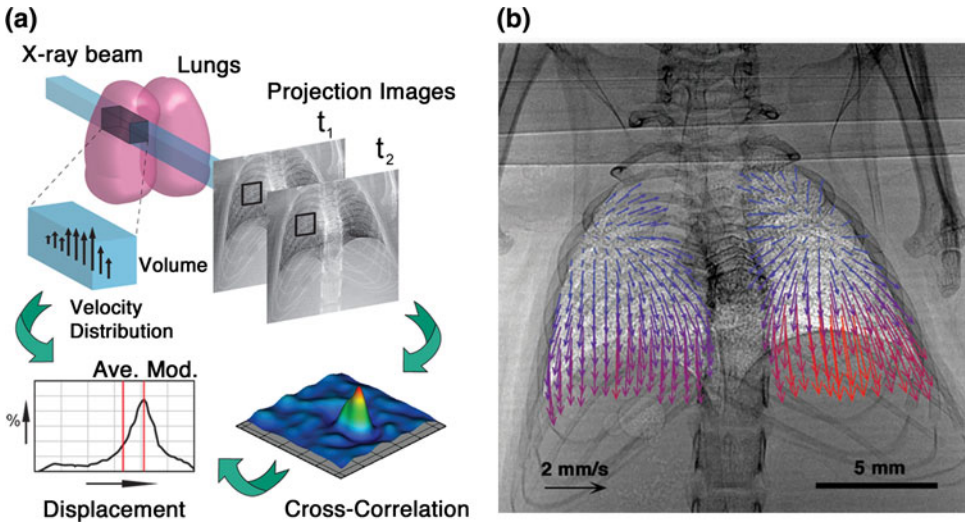

FIGURE 2. ***In vivo*** **detection of lung tissue motion. (a) Figure showing the 3D nature of X-ray illumination and velocimetric cross-correlation analysis. Each 2D sampling region in the projection images represents a 3D volume for which a distribution of velocities may be present. The present analysis selects the modal velocity, which may significantly differ from the mean. (b)** ***In vivo*** **detection of lung tissue motion. Instantaneous velocity of a healthy mouse lung, ~140 ms after start of inspiration, shown as a vector field. Vectors are reduced in number (293 of 2640 displayed) for clarity. Vectors are coloured according to magnitude (from lowest; blue, to highest; red) of velocity. The complete time sequence of inspiration consists of 70 instantaneous vector fields (media), one of which is shown.**

this is an established technique for measuring differential fluid velocities,[3] including blood flow.[21,38,41] PIV determines the movement of particles from one image to the next, yielding information on both velocity and direction of particle movement. The basic concept is demonstrated in Fig. 2a. Images are paired and discretised into small sub-regions and cross-correlations are performed between the sub-regions in consecutive images. The position of the maximum of the cross-correlation function determines the most common (modal) inter-frame displacement of the structures within each sub-region. Division of the displacement by the known inter-frame time yields the local modal velocity.

X-ray velocimetry has been utilised for the measurement of flow within channels,[23,25,32] for blood flow[10,24,33] and has recently been adapted to 3D analysis.[10,13,24] The high contrast intensity patterns produced by PCXI of the lung[26] can be used instead of having to introduce exogenous particles, as is the practice in conventional PIV. As a result, a comprehensive map displaying regional tissue velocities can be generated at all stages of the breathing cycle.

Whole animal motion was removed from image sequences by velocimetric analysis of upper vertebrae, followed by interpolation of images onto a static reference frame. Lungs were isolated from images by band-pass filtering using the appropriate image frequencies[19] and regions containing the lungs were identified and masked. Following this pre-processing, velocimetric analysis was conducted for 5 consecutive inspirations using customised software[11] and the data phase-averaged to produce data sets of 70 frames displaying the velocity vector fields throughout inspiration for each animal.

Divergence

At every time-point the spatial derivatives of the velocity fields can be evaluated[12] and summed to form the two-dimensional divergence field.[12] The spatial derivative distinguishes between bulk displacement of tissue and regional variations in tissue displacement, highlighting local differences in motion between regions. These local differences are directly related to local tissue expansion, and hence local variations in the divergence could be considered to be a measure of heterogeneity of tissue expansion and, by implication, tissue properties. For the sake of clarity of expression this projected divergence in motion will hereafter simply be referred to as the divergence. The total divergence over inspiration is the sum of the divergence between each pair of subsequent time points. As the data are integrated over the entire inspiration, total divergence is represented in a single map.

Statistics

Unpaired one-tailed *t*-tests were used to compare mean tidal volume and histological parameters. Two-way repeated measures ANOVA was used to determine differences in frequency distributions of divergence and time of divergence. Results were considered statistically significant at $p < 0.05$. Values are reported as mean ± SEM (unless stated otherwise).

RESULTS

Physiological Analysis

Plethysmography was used to measure tidal volume (V_T) during both spontaneous breathing and mechanical ventilation. Lung compliance was assessed only during mechanical ventilation, as airway pressure measurements were not available during spontaneous breathing. At 36 h after bleomycin treatment, the spontaneous V_T was significantly increased from 1.4 ± 0.1 mL/kg in saline-treated mice to 1.9 ± 0.1 mL/kg in bleomycin-treated mice, whereas spontaneous breathing rates were reduced from 480 ± 38 to 283 ± 34 breaths/min. However, no significant differences in global lung compliance (0.68 ± 0.04 vs. 0.71 ± 0.10 mL/cmH_2O/kg) could be detected during mechanical ventilation (Figs. 3a and 3b). Similarly, at 6 days after bleomycin treatment, the spontaneous V_T remained significantly elevated (1.2 ± 0.1 vs. 1.6 ± 0.2 mL/kg) and the ventilation rate was reduced (440 ± 13 vs. 235 ± 40 breaths/min), but no significant affect on global lung compliance (0.50 ± 0.04 vs. 0.55 ± 0.05 mL/cmH_2O/kg) was detected during mechanical ventilation (Figs. 3c and 3d).

Histological Analysis

Lung regions displaying structural alterations were clearly evident at both 36 h and 6 days after bleomycin treatment (Figs. 4c–4e), with increased and abnormal collagen deposition, reduced airway dimensions and peri-alveolar wall thickening. These abnormal changes were localised, occupying only 11.1 ± 0.5% of lung tissue at 6 days, and were distributed between large regions of normal tissue (Fig. 4). As a result, a subset analysis was performed,[22] to separately analyse normal and abnormal regions of lung tissue in bleomycin-treated mice. The relative volume density of parenchymal lung tissue was increased from 36.8 ± 3.6% in normal regions to 48.9 ± 1.5% in abnormal regions of lung tissue.

Velocimetry

Determined using X-ray velocimetry, the velocity vectors define the timing and extent of regional lung

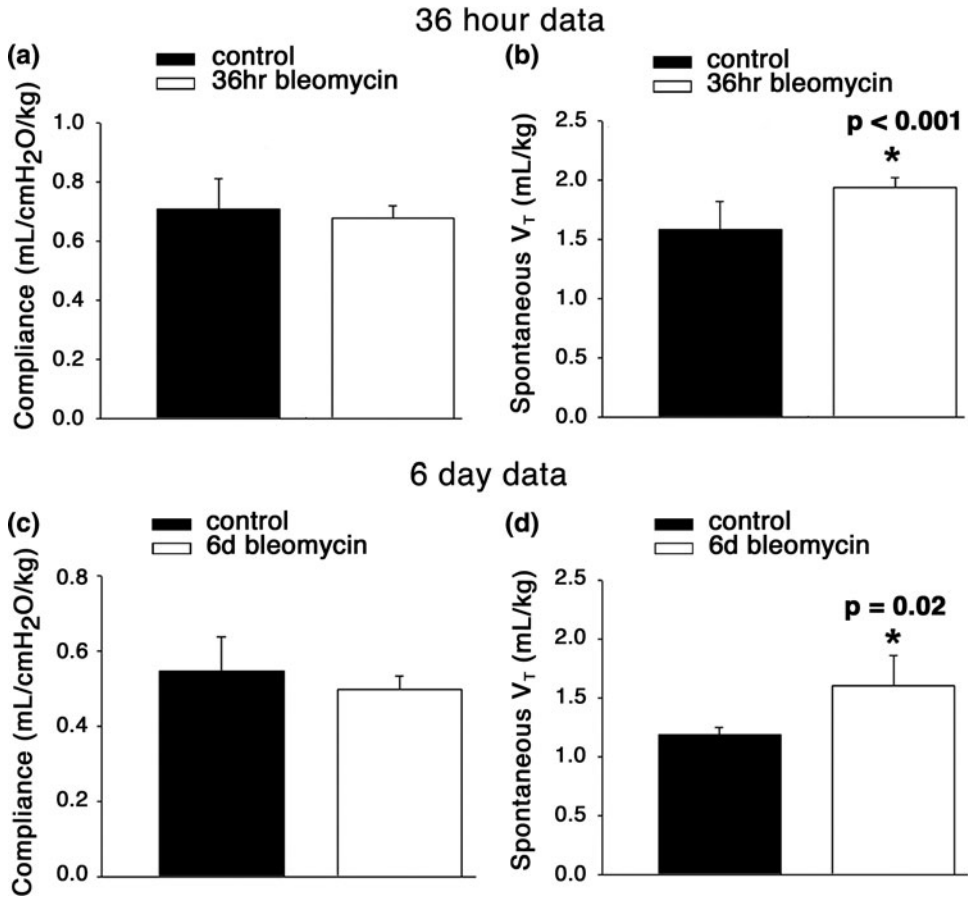

FIGURE 3. Physiological measures of lung pathology comparing controls with groups 36 h after bleomycin exposure and 6 days after exposure. Comparisons of the compliance for treated groups with controls (statistically insignificant) at (a) 36 h and (c) 6 days after treatment. Comparisons of the spontaneous tidal volumes (V_T) at (b) 36 h and (d) 6 days after treatment. Tidal volumes in controls are significantly lower than treated groups but are non specific and global in nature.

motion throughout a breath. The vectors measured at mid-inspiration demonstrate that regional lung motion is very heterogeneous (Fig. 2) at this point in the breathing cycle. The heterogeneous nature of regional lung motion throughout the breathing cycle is shown in the movie, which also demonstrates the changing dynamic of the velocity vector field (Movie 1).

Divergence—Validation

To validate the divergence analysis, an existing, published, PCXI image data set[28] was evaluated using the divergence analysis outlined in this work. In that work, PCXI images were acquired as rabbit foetus lungs were slowly ventilated for their first breaths (*in situ*) inside a water plethysmograph—allowing concurrent measurements of lung air volume as it rises from 0.

The PCXI images were analysed for velocimetry and divergence. The divergence data was then integrated throughout the entire series rather than just each breath and compared to the plethysmograph data. A scatter-plot of the integrated divergence (Fig. 5a) plotted against the lung volume as measured by water plethysmograph shows strong correlation between the two quantities ($R^2 = 0.98$). The gradient of the line of best-fit could be considered as a combination of the image magnification (pixel size) and an equivalent thickness of the lung since this gradient represents the empirically determined conversion factor to convert between the change in area (in pixels) and a change in volume (mL). To demonstrate the direct relationship between these quantities, the divergence data has been normalised by the empirical thickness and plotted (Fig. 5b) with the lung volume as measured by water plethysmography against time. Despite some minor inaccuracies brought about by the imperfect sealing of the animal in the water plethysomgraph and the two-dimensional nature of the image data, the excellent agreement between these data demonstrates the direct link between divergence and tissue expansion and hence tissue mechanical properties.

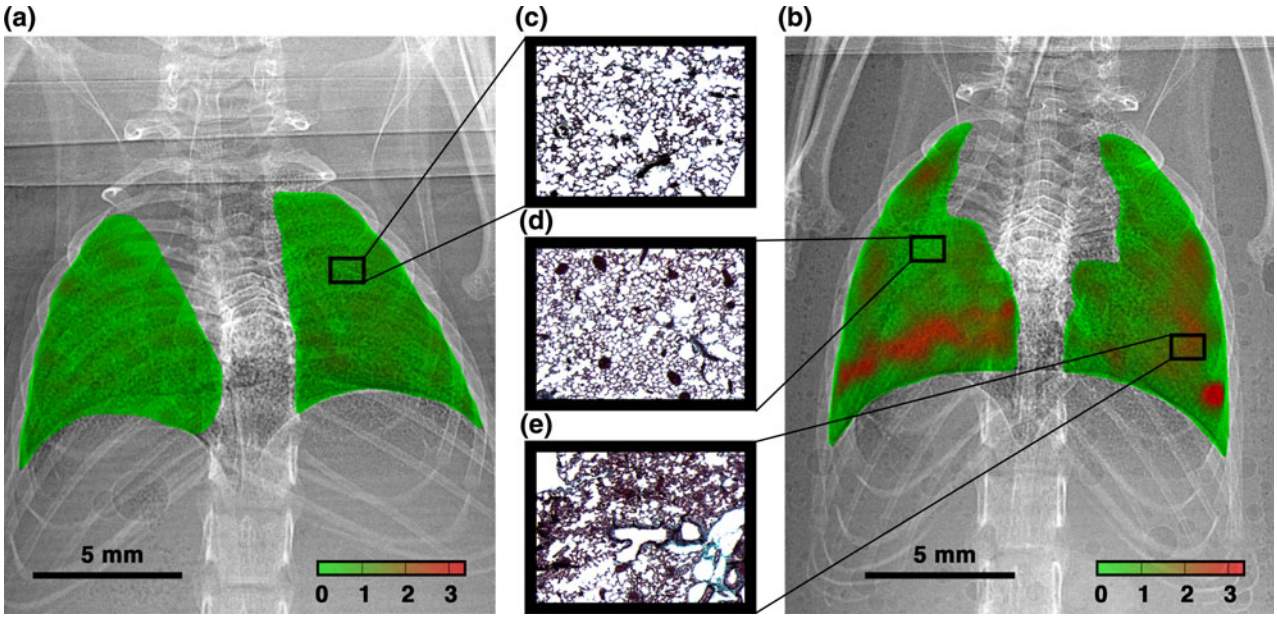

FIGURE 4. Regional divergence within the lung and matching histology. (a), (b) Colour maps of regional divergence determined using X-ray velocimetry for typical: (a) control and (b) bleomycin-treated mice (6 days after exposure). Data are normalised by the average divergence across the control group and colour maps generated using the same colour-scale (see legend). The mice treated with bleomycin (b) have dramatic regional alterations in the pattern of divergence. Histological image (c) from lung imaged in (a) is typical of the control group. Histological images (d, e) from lung imaged in (b) are typical of the pathological group 6 days after bleomycin treatment. Treated lungs show both regions of healthy tissue (d) and localised regions that are both hypercellular and endatemous (e).

Divergence—Bleomycin Treatment

Divergence data for bleomycin treated mice and controls were normalised by the average of controls and accumulated into frequency distribution curves, demonstrating that major differences ($p < 0.001$) in regional lung motion can be detected between saline-treated and bleomycin-treated mice at both 36 h and 6 days after treatment. Frequency distribution curves (Fig. 6a) show that divergence, within individual regions of lung tissue, was on average 24% greater in bleomycin-treated mice compared to saline-treated controls at 36 h after treatment, despite having the same global V_T. Moreover, in bleomycin-treated mice at 36 h after treatment, 14% of lung regions showed local differences twice the mean value in saline-treated controls; less than 5% of lung regions showed this degree of divergence in control mice, indicating a three-fold increase between bleomycin-treated and control mice.

At 6 days after bleomycin treatment, the changes in lung motion were more enhanced than those detected at 36 h after treatment. Indeed, despite no changes in global lung compliance, X-ray velocimetry detected a highly significant shift in the frequency distribution curve towards greater divergence (Fig. 6b). On average, the divergence of individual lung regions was 76% greater in bleomycin-treated mice compared to saline-treated controls. Furthermore, 47% of lung regions in treated mice showed local differences in motion twice the mean value of saline-treated mice, while less than 4% of lung regions showed this degree of divergence in saline-treated mice. Hence, there is nearly a 12-fold difference in divergence between bleomycin-treated mice and controls at 6 days after treatment. From these data, regional maps of divergence can be reconstructed and superimposed on the lung image to identify regions with abnormal motion (Fig. 4).

DISCUSSION

Although ventilators, plethysmographs and spirometers can measure many characteristics of lung function, those measures reflect the integrated average of the entire lung. As a result, these techniques have limited ability to detect regional lung disease until it is sufficiently widespread to influence total lung function. In contrast, we have demonstrated the capability of X-ray velocimetry to non-invasively detect breath-by-breath alterations in regional lung motion that occur even during the early stages of lung disease. Importantly, the velocimetric technique offers the advantages of detecting regional changes in lung function early, accurately and most importantly, *in situ*.

Superposition of the lung tissue velocity maps over the phase-contrast images acquired at mid-inspiration (140 ms after inspiration onset) clearly demonstrates

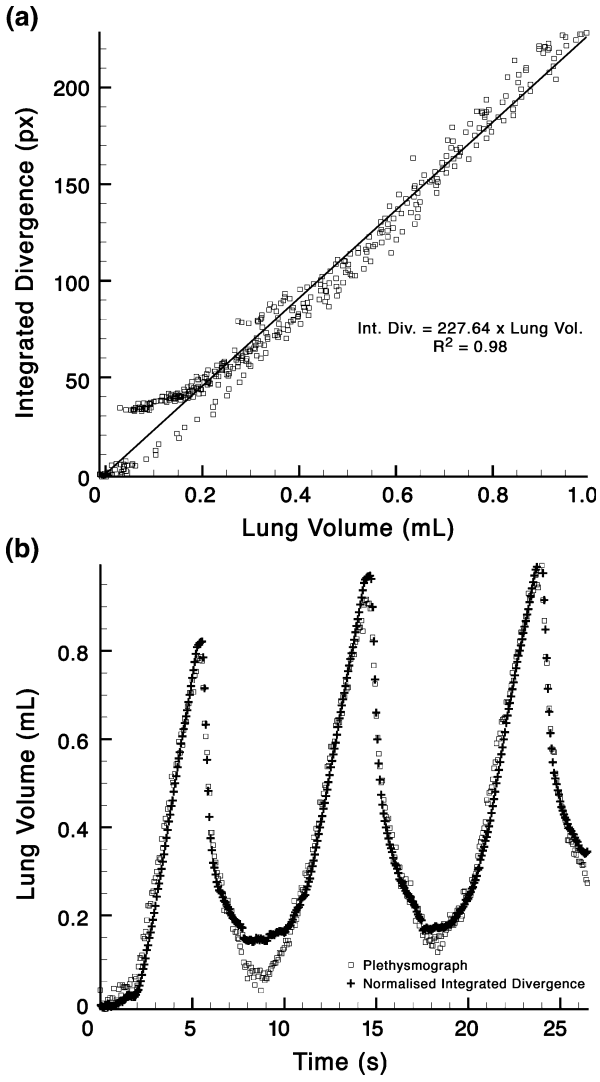

FIGURE 5. Empirical relationship between lung divergence and tissue expansion. (a) Scatter-plot of divergence (integrated throughout entire data series) and lung volume (measured by water plethysmography) of a rabbit measured from its first breath. The solid line indicates a line of best fit, with an $R^2 = 0.98$ indicating excellent correlation between the data sets. (b) Time-series of lung volume (measured by water plethysmography) co-plotted with divergence (integrated throughout the entire data series and normalised by the co-efficient determined by the fit in (a)).

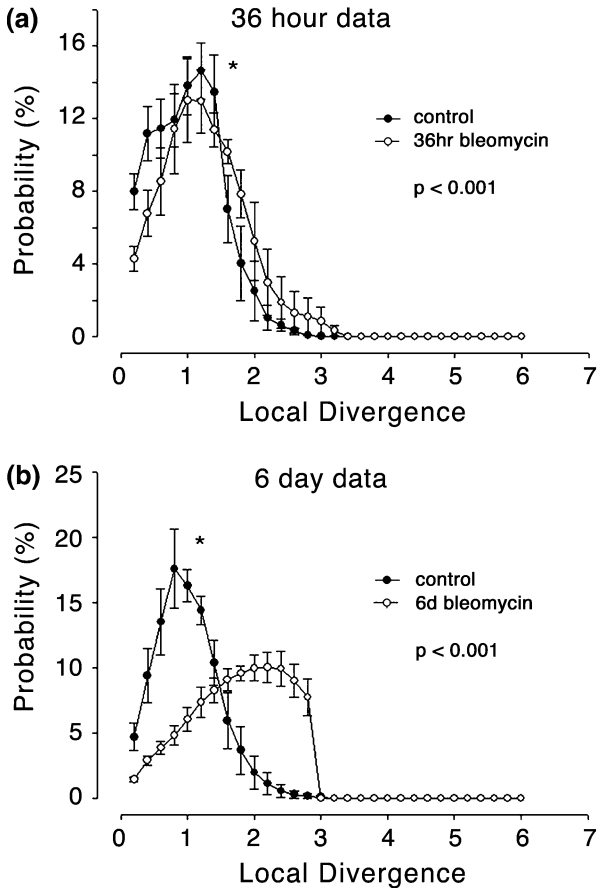

FIGURE 6. Velocimetric measures of lung pathology comparing controls with groups 36 h and 6 days after bleomycin exposure. Frequency distribution of the divergence (normalised to the average of controls) is compared for treated groups ($n = 4$) with controls ($n = 3$). Data are normalised by the average of the controls. (a) At 36 h post treatment, treated mice have 24% greater divergence on average and 14% of treated lungs show differences ×2 the control average compared with less than 5% for control lungs. (b) At 6 days post treatment, treated mice have 76% greater divergence on average and 47% of treated lungs show differences ×2 the control average compared with less than 4% for control lungs.

the heterogeneity of lung motion (Fig. 2). Combining consecutive images into a movie (Movie 1) reveals the changing dynamic of the velocity vector field during a breath and demonstrates that regional lung tissue motion is complex and non-linear. Indeed, regional velocities are most likely influenced by local characteristics of regional compliance, the compliance and motion of nearby tissue, as well as the proximity to structures such as the diaphragm, heart and chest wall. For example, lung tissue near the diaphragm displayed significantly more motion than tissue near the apex of the lung (Fig. 2b), which is likely due to differences in compliance as well as motion and activity of the chest wall that is immediately adjacent to the lung tissue. To accommodate the large differential in normal motion across the lung, a functional measure was derived from the velocity fields to identify regions with abnormal motion potentially caused by disease. Specifically, we calculated the local divergence normalised to the average for all controls for each treatment period (e.g., 36 h or 6 days) so that differences could be detected.

Our measure of divergence is derived from integration of the velocity vector field within each region over an entire breath. It is well understood that the divergence of a velocity field relates to the local expansion or contraction of the object, which in this case is lung tissue.[9] As such the divergence accounts for normal variations in tissue motion (such as the increased

motion near to the diaphragm compared to the apex) and converts heterogeneous patterns of tissue motion (displayed by normal tissue) to a homogenous pattern of divergence. However, we anticipate heterogenous regions of tissue properties (either resistance or compliance) to result in local variations in divergence.

However, lung tissue motion is three-dimensional and our divergence measures are two-dimensional. Therefore, the most correct interpretation of our measure of divergence is that it directly relates to local heterogeneity of lung tissue motion caused by differences in expansion. If all ventilation parameters, such as inflation times, pressures and gas flows are kept constant, this local heterogeneity in motion reflects differences in the mechanical response of lung tissue across the lung. This altered response must be due to either changes in the tissue mechanical properties, or a constriction/dilation of the airways leading to local alteration in resistance or compliance.

To test the ability of X-ray velocimetry and our subsequent analysis to detect abnormal lung motion, we exposed mice to bleomycin, which results in progressive lung injury.[31] Inhaled bleomycin is a well characterised and commonly used experimental model of pulmonary fibrosis that begins with the initiation of an inflammatory cascade.[2] Since Balb/c nude mice (an immuno-deficient strain) were utilised in the current study, it is not surprising that the pulmonary fibrotic response was reduced in these mice compared with reports in other strains.[52] This is likely because inflammatory responses are reduced in these mice,[44] although a recent study has also observed a similar reduced response in conventional Balb/c mice.[37] In any event, it is apparent that the induced pathological changes were insufficient to affect global lung compliance at the time points measured in this study, as observed previously in conventional Balb/c mice.[37] We deliberately examined the mice at 36 h and 6 days after treatment, which encompasses the early stages of disease pathogenesis, when the induced changes can be detected histologically but not physiologically.[37] Indeed, a previous study has indicated that the maximum response to bleomycin occurs at 21 days for conventional Balb/c mice, which is the only time that functional changes can be detected.[37] However, it is clear from the histological analysis (Fig. 4), that the bleomycin treatment was sufficient to cause observable focal lesions within lung tissue.

Our velocimetric analysis in bleomycin-treated mice revealed highly significant changes in regional lung motion compared to saline-treated mice. Despite having similar tidal volumes and inflation pressures during mechanical ventilation (indicating no change in global compliance), bleomycin treatment increased divergence across the lung by 24% at 36 h and by 76% at 6 days. This highly sensitive measure yielded a three-fold difference between the groups after only 36 h of treatment and was increased further after 6 days of treatment.

It is of interest that we could not detect a change in global lung compliance during mechanical ventilation at either 36 h or 6 days after treatment, but that tidal volumes during spontaneous breathing were significantly increased by bleomycin treatment at both times (Fig. 3). The higher tidal volumes during spontaneous breathing were partially matched with lower ventilation rates resulting in minute ventilation (mL/min/kg) values that were slightly reduced but statistically similar in bleomycin and saline-treated mice.

In summary, this study demonstrates that PCXI combined with velocimetry can measure regional lung motion and define the regional velocity changes at each stage of the respiratory cycle. Our results demonstrate that despite the large heterogeneity in normal motion across the lung, a detailed analysis of the velocity vectors can provide a very sensitive method for detecting abnormal motion caused by respiratory disease.

ELECTRONIC SUPPLEMENTARY MATERIAL

The online version of this article (doi: 10.1007/s10439-011-0493-0) contains supplementary material, which is available to authorized users.

ACKNOWLEDGMENTS

We thank Charlene Chua for assistance with figures; Melissa Siew for assistance with statistical analysis; David Paganin, Kevin Wheeler, John McDougal, Bruce Thompson and Christopher Stuart-Andrews for discussions. Research is funded by the Australian Research Council (DP110101498), the National Health and Medical Research Council (491103) and supported by beamtime grants from the Japan Synchrotron Radiation Research Institute. We acknowledge travel funding provided by the International Synchrotron Access Program (ISAP) managed by the Australian Synchrotron and funded by the Australian Government.

REFERENCES

[1]Adam, J. F., *et al*. Quantitative functional imaging and kinetic studies with high-Z contrast agents using synchrotron radiation computed tomography. *Clin. Exp. Pharmacol. Physiol.* 36(1):95–106, 2009.

[2]Adamson, I. Y. R., and D. H. Bowden. Pathogenesis of bleomycin-induced pulmonary fibrosis in mice. *Am. J. Pathol.* 77(2):185–199, 1974.

[3]Adrian, R. J. Twenty years of particle image velocimetry. *Exp. Fluids* 39(2):159–169, 2005.
[4]Albert, S. P., *et al.* The role of time and pressure on alveolar recruitment. *J. Appl. Physiol.* 106(3):757–765, 2009.
[5]Allen, G. B., *et al.* Pulmonary impedance and alveolar instability during injurious ventilation in rats. *J. Appl. Physiol.* 99(2):723–730, 2005.
[6]Black, C. L. B., *et al.* Relationship between dynamic respiratory mechanics and disease heterogeneity in sheep lavage injury. *Crit. Care Med.* 35(3):870–878, 2007.
[7]Boulet, L. P., M. Belanger, and G. Carrier. Airway responsiveness and bronchial-wall thickness in asthma with or without fixed air-flow obstruction. *Am. J. Respir. Crit. Care Med.* 152(3):865–871, 1995.
[8]Castillo, R., *et al.* Ventilation from four-dimensional computed tomography: density versus Jacobian methods. *Phys. Med. Biol.* 55(16):4661–4685, 2010.
[9]Christensen, G. E., *et al.* Tracking lung tissue motion and expansion/compression with inverse consistent image registration and spirometry. *Med. Phys.* 34(6):2155–2163, 2007.
[10]Dubsky, S., *et al.* Computed tomographic X-ray velocimetry. *Appl. Phys. Lett.* 96(2):023702, 2010.
[11]Fouras, A., D. Lo Jacono, and K. Hourigan. Target-free Stereo PIV: a novel technique with inherent error estimation and improved accuracy. *Exp. Fluids* 44(2):317–329, 2008.
[12]Fouras, A., and J. Soria. Accuracy of out-of-plane vorticity measurements derived from in-plane velocity field data. *Exp. Fluids* 25(5–6):409–430, 1998.
[13]Fouras, A., *et al.* Three-dimensional synchrotron X-ray particle image velocimetry. *J. Appl. Phys.* 102(6):064916, 2007.
[14]Guerrero, T., *et al.* Quantification of regional ventilation from treatment planning CT. *Int. J. Radiat. Oncol. Biol. Phys.* 62(3):630–634, 2005.
[15]Guerrero, T., *et al.* Dynamic ventilation imaging from four-dimensional computed tomography. *Phys. Med. Biol.* 51(4):777–791, 2006.
[16]Hodgson, M. J., D. K. Parkinson, and M. Karpf. Chest X-rays in hypersensitivity pneumonitis—a metaanalysis of secular trend. *Am. J. Ind. Med.* 16(1):45–53, 1989.
[17]Hoffman, E. A., *et al.* Estimation of regional pleural surface expansile forces in intact dogs. *J. Appl. Physiol.* 55(3):935–948, 1983.
[18]Hogg, J. C. Pathophysiology of airflow limitation in chronic obstructive pulmonary disease. *Lancet* 364(9435): 709–721, 2004.
[19]Hooper, S. B., *et al.* Imaging lung aeration and lung liquid clearance at birth. *FASEB J.* 21(12):3329–3337, 2007.
[20]Hooper, S. B., *et al.* Imaging lung aeration and lung liquid clearance at birth using phase contrast X-ray imaging. *Clin. Exp. Pharmacol. Physiol.* 36(1):117–125, 2009.
[21]Hove, J. R., *et al.* Intracardiac fluid forces are an essential epigenetic factor for embryonic cardiogenesis. *Nature* 421(6919):172–177, 2003.
[22]Hsia, C. C. W., *et al.* An official research policy statement of the American Thoracic Society/European Respiratory Society: standards for quantitative assessment of lung structure. *Am. J. Respir. Crit. Care Med.* 181(4):394–418, 2010.
[23]Im, K. S., *et al.* Particle tracking velocimetry using fast X-ray phase-contrast imaging. *Appl. Phys. Lett.* 90(9):3, 2007.
[24]Irvine, S. C., *et al.* Phase retrieval for improved three-dimensional velocimetry of dynamic X-ray blood speckle. *Appl. Phys. Lett.* 93(15):153901, 2008.
[25]Jamison, R. A., *et al.* X-ray velocimetry and haemodynamic forces within a stenosed femoral model at physiological flow rates. *Ann. Biomed. Eng.* 39(6):1643–1653, 2011.
[26]Kitchen, M. J., *et al.* On the origin of speckle in X-ray Phase Contrast images of lung tissue. *Phys. Med. Biol.* 49(18):4335–4348, 2004.
[27]Kitchen, M. J., *et al.* Phase contrast X-ray imaging of mice and rabbit lungs: a comparative study. *Br. J. Radiol.* 78(935):1018–1027, 2005.
[28]Kitchen, M. J., *et al.* Dynamic measures of regional lung air volume using Phase Contrast X-ray Imaging. *Phys. Med. Biol.* 53(21):6065–6077, 2008.
[29]Kitchen, M. J., *et al.* A new design for high stability pressure-controlled ventilation for small animal lung imaging. *J. Instrum.* 5:T02002, 2010.
[30]Lai-Fook, S. J., and R. E. Hyatt. Effects of age on elastic moduli of human lungs. *J. Appl. Physiol.* 89(1):163–168, 2000.
[31]Lazenby, A. J., *et al.* Remodeling of the lung in bleomycin-induced pulmonary fibrosis in the rat—an immunohistochemical study of laminin, type-IV collagen, and fibronectin. *Am. Rev. Respir. Dis.* 142(1):206–214, 1990.
[32]Lee, S. J., and G. B. Kim. X-ray particle image velocimetry for measuring quantitative flow information inside opaque objects. *J. Appl. Phys.* 94(5):3620–3623, 2003.
[33]Lee, S. J., and G. B. Kim. Synchrotron microimaging technique for measuring the velocity fields of real blood flows. *J. Appl. Phys.* 97(6):6, 2005.
[34]Lewis, R. A. Medical phase contrast x-ray imaging: current status and future prospects. *Phys. Med. Biol.* 49(16):3573–3583, 2004.
[35]Lewis, R. A., *et al.* Dynamic imaging of the lungs using X-ray phase contrast. *Phys. Med. Biol.* 50(21):5031–5040, 2005.
[36]Maltais, F., *et al.* Comparison of static and dynamic measurements of intrinsic peep in mechanically ventilated patients. *Am. J. Respir. Crit. Care Med.* 150(5):1318–1324, 1994.
[37]Manali, E., *et al.* Static and dynamic mechanics of the murine lung after intratracheal bleomycin. *BMC Pulm. Med.* 11(1):33, 2011.
[38]Nesbitt, W. S., *et al.* A shear gradient-dependent platelet aggregation mechanism drives thrombus formation. *Nat. Med.* 15(6):665–673, 2009.
[39]Onodera, M., *et al.* Determination of ventilatory volume in mice by whole body plethysmography. *Jpn. J. Physiol.* 47(4):317–326, 1997.
[40]Pan, T., *et al.* 4D-CT imaging of a volume influenced by respiratory motion on multi-slice CT. *Med. Phys.* 31(2): 333–340, 2004.
[41]Poelma, C., *et al.* In vivo blood flow and wall shear stress measurements in the vitelline network. *Exp. Fluids* 45(4):703–713, 2008.
[42]Reinhardt, J. M., *et al.* Registration-based estimates of local lung tissue expansion compared to xenon CT measures of specific ventilation. *Med. Image Anal.* 12(6):752–763, 2008.
[43]Robertson, H. T., *et al.* High-resolution maps of regional ventilation utilizing inhaled fluorescent microspheres. *J. Appl. Physiol.* 82(3):943–953, 1997.
[44]Schrier, D. J., S. H. Phan, and B. M. McGarry. The effects of the nude (nu/nu) mutation on bleomycin-induced pulmonary fibrosis—a biochemical evaluation. *Am. Rev. Respir. Dis.* 127(5):614–617, 1983.

[45]Sethi, S., and T. F. Murphy. Current concepts: infection in the pathogenesis and course of chronic obstructive pulmonary disease. *N. Engl. J. Med.* 359(22):2355–2365, 2008.
[46]Siew, M. L., *et al.* Inspiration regulates the rate and temporal pattern of lung liquid clearance and lung aeration at birth. *J. Appl. Physiol.* 106(6):1888–1895, 2009.
[47]Snigirev, A., *et al.* On the possibilities of X-ray phase contrast microimaging by coherent high-energy synchrotron radiation. *Rev. Sci. Instrum.* 66(12):5486–5492, 1995.
[48]Sundaram, T. A., and J. C. Gee. Towards a model of lung biomechanics: pulmonary kinematics via registration of serial lung images. *Med. Image Anal.* 9(6):524–537, 2005.
[49]Sznitman, J., *et al.* Visualization of respiratory flows from 3D reconstructed alveolar airspaces using X-ray tomographic microscopy. *J. Vis.* 13(4):337–345, 2010.
[50]Tustison, N. J., *et al.* Pulmonary kinematics from tagged hyperpolarized helium-3 MRI. *J. Magn. Reson. Imaging* 31(5):1236–1241, 2010.
[51]Tustison, N. J., *et al.* Pulmonary kinematics from image data: a review. *Acad. Radiol.* 18(4):402–417, 2011.
[52]Udalov, S., *et al.* Effects of phosphodiesterase 4 inhibition on bleomycin-induced pulmonary fibrosis in mice. *BMC Pulm. Med.* 10:26, 2010.
[53]Westneat, M. W., J. J. Socha, and W.-K. Lee. Advances in biological structure, function, and physiology using synchrotron X-ray imaging. *Annu. Rev. Physiol.* 70:119–142, 2008.
[54]Westneat, M. W., *et al.* Tracheal respiration in insects visualized with synchrotron X-ray imaging. *Science* 299(5606):558–560, 2003.
[55]Wilkins, S. W., *et al.* Phase-contrast imaging using polychromatic hard X-rays. *Nature* 384(6607):335–338, 1996.
[56]Yagi, N., *et al.* Refraction-enhanced X-ray imaging of mouse lung using synchrotron radiation source. *Med. Phys.* 26(10):2190–2193, 1999.
[57]Yin, Y. B., *et al.* Simulation of pulmonary air flow with a subject-specific boundary condition. *J. Biomech.* 43(11): 2159–2163, 2010.